

# Tracking Electron Uptake from a Cathode into *Shewanella* Cells: Implications for Energy Acquisition from Solid-Substrate Electron Donors

Annette R. Rowe,<sup>a</sup> Pournami Rajeev,<sup>a</sup> Abhiney Jain,<sup>b,c</sup> Sahand Pirbadian,<sup>d</sup> Akihiro Okamoto,<sup>e</sup> Jeffrey A. Gralnick,<sup>b,c</sup> Mohamed Y. El-Naggar,<sup>d,f,g</sup> Kenneth H. Nealson<sup>a,f</sup>

<sup>a</sup>Department of Earth Sciences, University of Southern California, Los Angeles, California, USA

<sup>b</sup>Department of Microbiology, University of Minnesota, St. Paul, Minnesota, USA

<sup>c</sup>BioTechnology Institute, University of Minnesota, St. Paul, Minnesota, USA

<sup>d</sup>Department of Physics and Astronomy, University of Southern California, Los Angeles, California, USA

<sup>e</sup>Global Research Center for Environment and Energy Based on Nanomaterials Science, National Institute for Materials Science (NIMS), Tsukuba, Ibaraki, Japan

<sup>f</sup>Department of Biological Sciences, University of Southern California, Los Angeles, California, USA

<sup>g</sup>Department of Chemistry, University of Southern California, Los Angeles, California, USA

**ABSTRACT** While typically investigated as a microorganism capable of extracellular electron transfer to minerals or anodes, *Shewanella oneidensis* MR-1 can also facilitate electron flow from a cathode to terminal electron acceptors, such as fumarate or oxygen, thereby providing a model system for a process that has significant environmental and technological implications. This work demonstrates that cathodic electrons enter the electron transport chain of *S. oneidensis* when oxygen is used as the terminal electron acceptor. The effect of electron transport chain inhibitors suggested that a proton gradient is generated during cathode oxidation, consistent with the higher cellular ATP levels measured in cathode-respiring cells than in controls. Cathode oxidation also correlated with an increase in the cellular redox (NADH/FMNH<sub>2</sub>) pool determined with a bioluminescence assay, a proton uncoupler, and a mutant of proton-pumping NADH oxidase complex I. This work suggested that the generation of NADH/FMNH<sub>2</sub> under cathodic conditions was linked to reverse electron flow mediated by complex I. A decrease in cathodic electron uptake was observed in various mutant strains, including those lacking the extracellular electron transfer components necessary for anodic-current generation. While no cell growth was observed under these conditions, here we show that cathode oxidation is linked to cellular energy acquisition, resulting in a quantifiable reduction in the cellular decay rate. This work highlights a potential mechanism for cell survival and/or persistence on cathodes, which might extend to environments where growth and division are severely limited.

**IMPORTANCE** The majority of our knowledge of the physiology of extracellular electron transfer derives from studies of electrons moving to the exterior of the cell. The physiological mechanisms and/or consequences of the reverse processes are largely uncharacterized. This report demonstrates that when coupled to oxygen reduction, electrode oxidation can result in cellular energy acquisition. This respiratory process has potentially important implications for how microorganisms persist in energy-limited environments, such as reduced sediments under changing redox conditions. From an applied perspective, this work has important implications for microbially catalyzed processes on electrodes, particularly with regard to understanding models of cellular conversion of electrons from cathodes to microbially synthesized products.

**Received** 18 December 2017 **Accepted** 21 December 2017 **Published** 27 February 2018

**Citation** Rowe AR, Rajeev P, Jain A, Pirbadian S, Okamoto A, Gralnick JA, El-Naggar MY, Nealson KH. 2018. Tracking electron uptake from a cathode into *Shewanella* cells: implications for energy acquisition from solid-substrate electron donors. *mBio* 9:e02203-17. <https://doi.org/10.1128/mBio.02203-17>.

**Editor** Markus W. Ribbe, University of California, Irvine

**Copyright** © 2018 Rowe et al. This is an open-access article distributed under the terms of the [Creative Commons Attribution 4.0 International license](https://creativecommons.org/licenses/by/4.0/).

Address correspondence to Annette R. Rowe, [annetrr@usc.edu](mailto:annetrr@usc.edu).

This work is C-DEBI contribution 417 and NAI-LU contribution 125.

**KEYWORDS** electron uptake, energy acquisition, reverse electron transport, *Shewanella*, systems biology

**E**lectromicrobiology involves extracellular electron transfer (EET) between solid-phase electron-active redox compounds and microorganisms. Study of these interactions using electrochemical techniques has provided fundamental insights into microbial physiology and spawned a variety of microbe-electrode-driven applied technologies (1–4). These applications include energy recovery from waste treatment, bioremediation, and, more recently, electrosynthesis—the conversion of electrical energy to microbially synthesized products (4). The mechanisms (and variations) of outward EET (utilized for the reduction of solid substrates) are well understood for two model systems, *Shewanella* and *Geobacter*. In contrast, little is known about the mechanisms of inward EET (utilized during the oxidation of solid substrates), even in these model systems. Because of this, the technological, ecological, and environmental implications of these microbially mediated processes remain poorly understood.

The mechanisms of EET from the interior of a cell to external electron acceptors have been extensively characterized in the gammaproteobacterial *Shewanella oneidensis* strain MR-1. Under anaerobic conditions with an organic acid electron donor and in the presence of a suitable sink for electrons on the cell exterior, electrons from the *S. oneidensis* MR-1 inner membrane quinone pool are transferred to the inner membrane-linked tetraheme cytochrome CymA (5, 6). Electron transfer to the cell exterior is thought to depend on protein-protein interactions between CymA and periplasmic electron-carrying proteins, such as the small tetraheme cytochrome (Cct) or the flavocytochrome fumarate reductase FccA (7–9). Cct and FccA likely interact with the Mtr EET respiratory pathway through MtrA, a periplasmic decaheme cytochrome (9). MtrA helps to traffic electrons across the outer membrane via interactions with the MtrB porin and with decaheme lipoprotein cytochromes (MtrC, OmcA) localized to the exterior of the outer membrane (10). These complexes (illustrated in Fig. 1A) have been shown to be involved in electron transfer (either directly or indirectly) to solid substrates, such as solid-state electrodes, and manganese or iron (oxy)hydroxides (11).

It has been demonstrated that mineral-reducing microbes like *Shewanella*, as well as anode reduction, can facilitate cathodic reactions, i.e., the transference of electrons from an electrode to a more oxidized terminal electron acceptor (4, 12–15). Under anaerobic conditions in *S. oneidensis* MR-1, this process can be coupled to fumarate reduction and has been proposed to result from a reversal of the electron transport pathways that function in anode reductions (16, 17). Notably, this is consistent with the reversibility demonstrated by the electrochemical characterization of several multi-heme cytochromes (10). However, the potential for energy acquisition remains unclear, especially given the relatively small energetic gains from coupling the Mtr pathway to anaerobic terminal electron acceptors (16). Coupling cathode oxidation with oxygen reduction has been observed previously in other organisms (13, 14), though it has never been specifically reported in *S. oneidensis* MR-1. Thermodynamically, oxygen allows for a high relative energy gain compared with that of many terminal electron acceptors. However, it is unknown whether *S. oneidensis* MR-1 cells are able to couple electrons from an extracellular source to oxygen reduction in a way that allows the generation of a proton motive force (PMF). Given the highly enriched cytochrome network in *Shewanella*, it is plausible that nonspecific reduction reactions occur between cytochromes and oxygen, resulting in a catalytic reduction of oxygen without concomitant proton pumping. Conversely, reversing the EET pathway may result in electrons entering the cellular quinone pool and/or interacting with one or more of the inner membrane cytochromes in a way that allow electrons to flow into existing electron transport chain components and, ultimately, into one of the three terminal oxygen-reducing cytochrome reductases (i.e., into *cbb*<sub>3</sub>, *aa*<sub>3</sub>, or *bd*) (18).

To better understand energy acquisition by *S. oneidensis* MR-1 under cathodic conditions, we used an electrode to impose electron-donating redox potentials in an

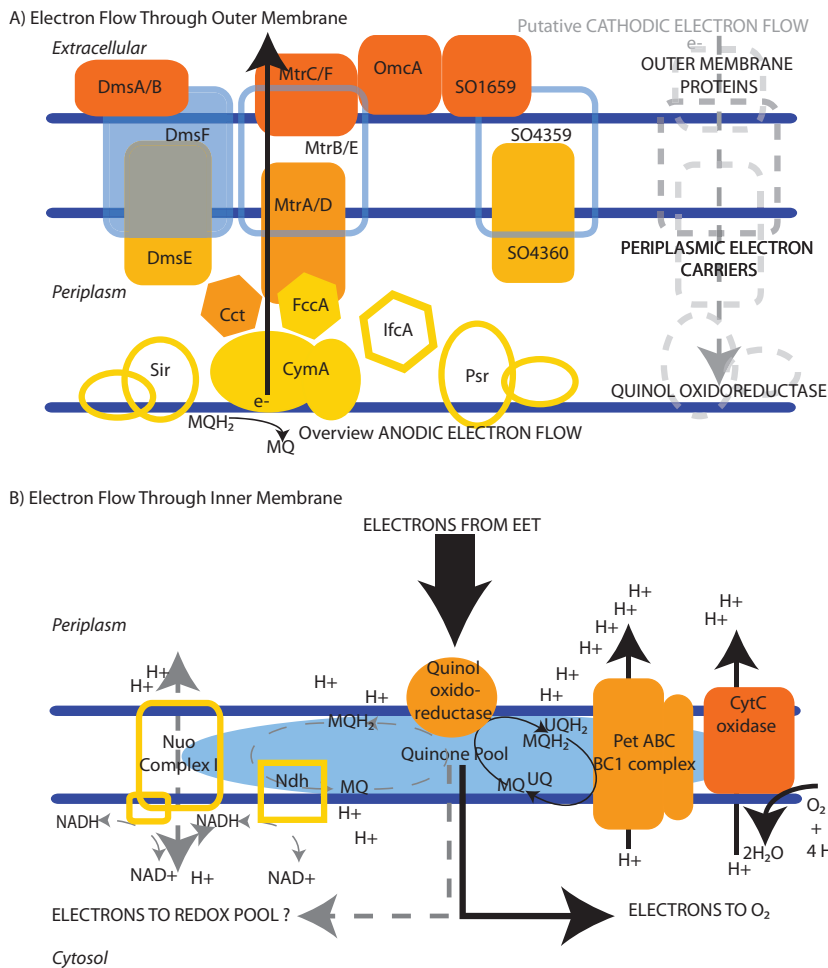


**FIG 1** Schematic representation of MR-1 membrane proteins potentially involved in cathodic electron flow. Traditional anodic electron flow is indicated via black arrows. The potential cytochromes and/or flavochromes involved in cathodic electron flow are illustrated. (A) The outer membranes of periplasmic components tested via mutant studies are diagrammed as filled shapes (details are listed in Table 1), and other known, though not tested, cytochrome-containing proteins are outlined. (B) The potential for reverse electron flow to NADH using proton motive force is also illustrated (via the reversibility of complex I-Nuo). Electron flow once electrons reach the inner membrane is diagrammed as passing from the quinone pool to a terminal cytochrome oxidase and eventually oxygen.

aerobic environment lacking exogenous organic carbon sources. Under these conditions, we set out to understand (i) whether or not electrons from a cathode that enter *S. oneidensis* MR-1 can be utilized for acquisition of cellular energy and (ii) what pathways are involved in electron flow from a cathode to oxygen. Understanding the physiology behind these biologically mediated cathodic processes may allow us to optimize and/or utilize microbes for various microbe-electrode applications, such as electrosynthesis, as well as to better understand microbial physiology under a variety of redox conditions.

**RESULTS**

**Electrons flow from a cathode to the *S. oneidensis* MR-1 cellular electron transport chain.** Oxygen-reducing cathode conditions were investigated in three-electrode electrochemical cells using working electrodes covered with a monolayer biofilm on indium-tin-doped oxide (ITO)-coated glass. Significantly more cathodic current was generated than under control conditions (abiotic/cell-free medium and killed-cell biomass) at voltages as high as  $-203$  mV compared to the voltage of a standard hydrogen electrode (SHE), and this effect was linked to the presence of

oxygen in *S. oneidensis* MR-1 monolayer cathode biofilms (see Fig. S1 in the supplemental material). Negative currents were observed in *S. oneidensis* MR-1 at potentials of up to  $-103$  mV versus the SHE (data not shown); however, the majority of experiments were run at  $-303$  mV to maintain a high signal-to-noise ratio over a range of experimental conditions. Notably, the redox potential of activities in these biofilms are several hundred millivolts higher than the experimentally observed redox potentials for electrochemical hydrogen production under these conditions ( $-550$  to  $-600$  mV versus the voltage of the SHE) and the theoretical standard redox potential for hydrogen at pH 7 ( $E^{\circ'} = -414$  mV versus the voltage of the SHE). Additionally, although *S. oneidensis* MR-1 contains hydrogenases and can grow anaerobically on hydrogen, these hydrogenases are not expressed and are thought to be inactive under oxic conditions (19, 20). Comparing the rates of electron flow between anodic ( $+397$  mV, anaerobic, 10 mM lactate) and cathodic ( $-303$  mV, aerobic, no exogenous electron donor) conditions for the same monolayer biofilms, cathodic conditions yielded on average  $23.7 \pm 5$  ( $n = 4$ ) times more current consumption than production. The possibility of these cathode-derived electrons entering the cellular electron transport chain (ETC) was investigated in this system using the combination of a redox active dye (RedoxSensor Green [RSG]) and ETC inhibitors. RSG is a lipid-soluble redox-active dye, previously shown to fluoresce in actively respiring aerobic and anaerobic microbial cells (21–23).

RSG fluoresces green when reduced, and active accumulation of the reduced dye within cells can be linked to respiratory conditions (i.e., active downhill electron flow through the ETC). While the specific oxidoreductases involved in RSG reduction are not known, previous work with *S. oneidensis* MR-1 investigated the effects of ETC inhibitors during aerobic growth on lactate and oxygen (21). Inhibition of RSG activity was seen when an ETC inhibitor was utilized; specifically, it was noted that inhibition of the electron flow at or prior to the terminal oxidase step also interfered with the cellular reduction of RSG (21). This suggests that interaction with a high-potential cytochrome is responsible for RSG reduction in *Shewanella*. Using UV fluorescence microscopy on transparent ITO electrodes, we quantified an increase in RSG fluorescence in *S. oneidensis* MR-1 cells under conditions of applied cathodic potential ( $-303$  mV versus the voltage of the SHE) in the presence of oxygen. Minimal fluorescence was observed under open-circuit conditions. The fluorescence signal seen under cathodic conditions was strongly inhibited by potassium cyanide, a respiration inhibitor (Fig. 2). These observations support the notion that an active cellular electron flow is required for active RSG reduction and accumulation in cells.

Time-lapse videos from these experiments demonstrate the rapid nature of this process; a marked increase in RSG signal intensity can be observed within 15 min of applying a cathodic potential (videos S1 to S3, available upon request). Additionally, RSG fluorescence significantly decreased within 15 min after addition of potassium cyanide, an inhibitor of cytochrome *c* oxidase (Fig. 2; videos S1 to S3, available upon request). Cathodic current was also mitigated by cyanide addition (between 67 and 78% loss of cathodic current) (Fig. 3), supporting a requirement for terminal cytochrome *c* oxidases to facilitate electron flow from a cathode. Removal of cyanide from a cathode biofilm after a 30-min exposure allowed for recovery of both the cathodic current (68% of the wild-type current was recovered) and RSG fluorescence, suggesting that this effect is due to the reversible inhibition of cytochrome *c* oxidases.

While cyanide is a general cytochrome oxidase inhibitor and several cytochrome oxidases have been shown to pump protons (24), inhibition at quinone proton translocation sites was also tested. Addition of antimycin A (an inhibitor of quinone oxidoreductases) also resulted in a rapid and marked decrease in cathodic current but had no effect on abiotic controls (Fig. 3). Notably, a 60 to 70% loss in cathodic current ( $[\text{cathodic current} - \text{inhibited current}]/\text{cathodic current}$ ) was observed within the first minute of inhibitor addition (Fig. 3). RSG activity was monitored in cathode biofilms under all inhibitor conditions. While a dissipation of fluorescence can still be observed using antimycin A (videos S4 to S6, available upon request), the quantification of RSG

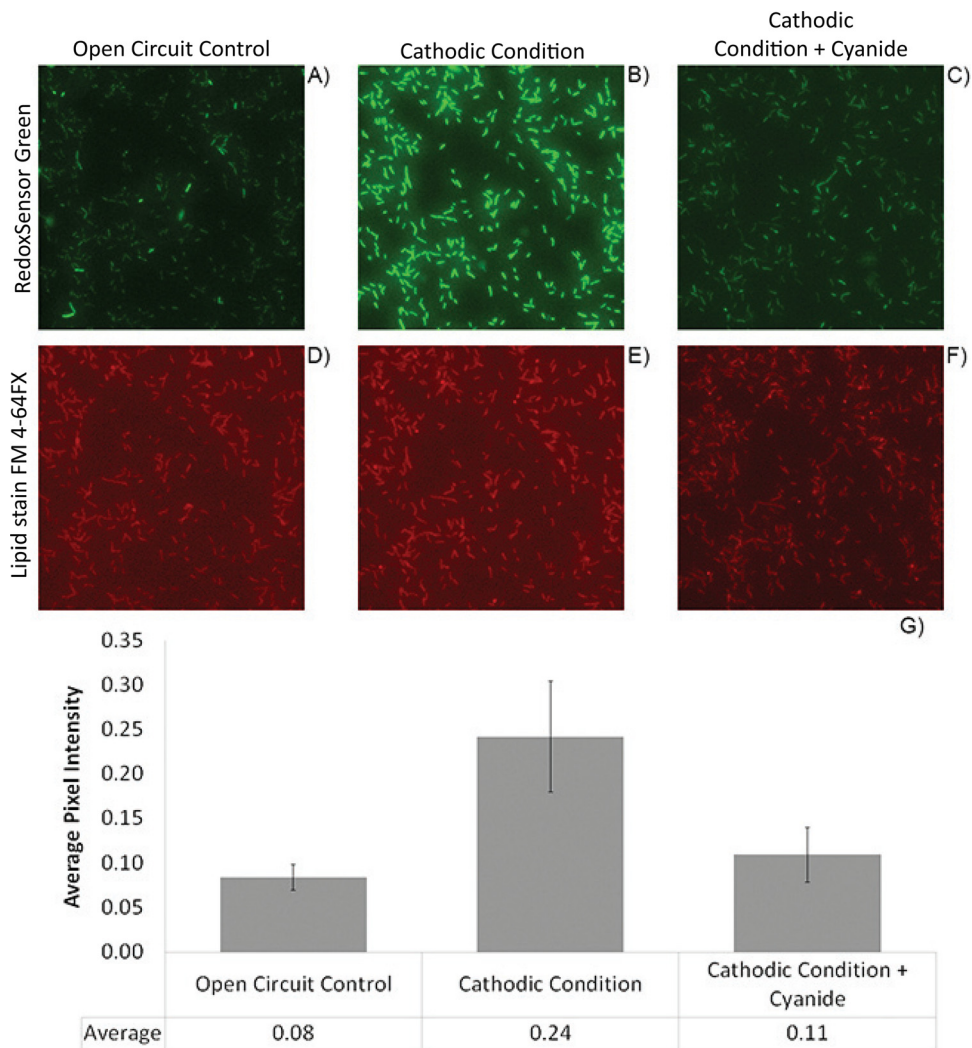


**FIG 2** RedoxSensor Green highlights electron flow through the cellular electron transport chain under cathodic conditions. (A to F) Representative images of MR-1 cells attached to ITO-coated glass and treated with RedoxSensor Green (A to C) and the lipid stain FM 4-64FX (D to F) are as described in Materials and Methods. Fluorescence intensities are compared between the control conditions (open circuit) (A and D), cathodic conditions ( $-303$  mV versus the voltage of the SHE) (B and E), and cathodic conditions with an inhibitor of cytochrome *c* oxidase added ( $-303$  mV versus the voltage of the SHE with 5 mM KCN added) (C and F). Average pixel intensity per cell was calculated for approximately 80 images for six time points per condition (average numbers of cells per image, 2,271, 1,904, and 2,234 for the control, cathodic, and inhibition conditions, respectively). Error bars indicate standard deviations in average pixel intensities (per population) per image (80 images were analyzed per experimental condition).

postaddition was made difficult by the autofluorescence of antimycin A. Though antimycin A, as a quinone mimic, may interact nonspecifically with other quinone oxidoreductases, it has been shown to preferentially inhibit the oxidation of ubiquinone by the cytochrome *bc<sub>1</sub>* complex in mitochondria (25). These results demonstrate that electron flow from a cathode passes through at least one coupling site in the cellular electron transport chain.

**Cellular energy carrier quantification in cathode-oxidizing *S. oneidensis* MR-1 cells.** To further investigate whether a proton gradient is generated under cathodic conditions that might consequently result in ATP generation, we measured pools of ATP and ADP within cathode biofilms. We compared the ATP/(ATP plus ADP) ratios (to normalize for differing overall cellular nucleotide levels) for replicate biofilms exposed to either cathodic conditions ( $-303$  mV versus the voltage of the SHE), cathodic conditions plus treatment with the protonophore uncoupler carbonyl



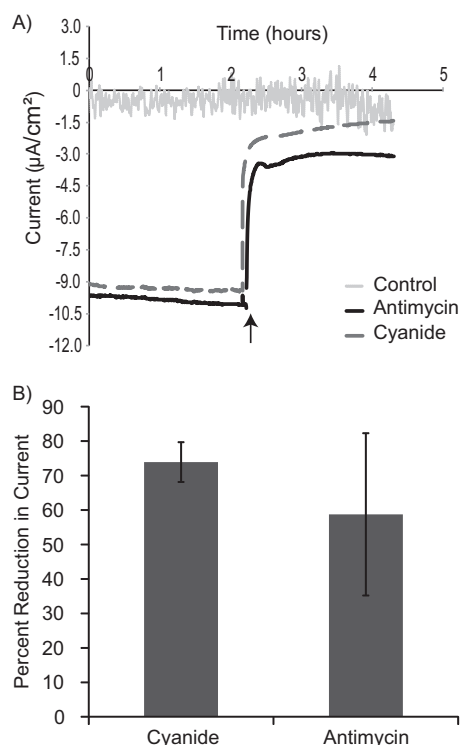


**FIG 3** The cathodic current is inhibited by cyanide addition. (A) Sample chronoamperometry plots for MR-1 cells attached to a cathode (results of one of three experiments are shown) and a cell-free control electrode ( $-303$  mV versus the voltage of the SHE), with addition of the electron transport chain inhibitors potassium cyanide ( $5$  mM) and antimycin A ( $20$   $\mu\text{M}$ ) (addition is indicated by the arrow), which inhibit cytochrome *c* oxidase and quinone oxidoreductases, respectively. The control sample was treated with both potassium cyanide and antimycin A at the time indicated. (B) The average percentages of reduction in cathodic current [(average cathodic current 1 h preinhibition) – the average cathodic current 1 h postinhibition]/average cathodic current 1 h preinhibition when electron transport chain inhibitors were added are illustrated for 3 reactors. The average total (100%) current for all experiments before inhibitor addition was  $-6.9 \pm 2.7$   $\mu\text{A}/\text{cm}^2$ . Error bars represent 1 standard deviation from results of triplicate experiments.

cyanide *m*-chlorophenyl hydrazine (CCCP) for 3 h, and poised potential conditions ( $197$  mV versus the voltage of the SHE) where minimal anodic current flow was observed (average of five replicates,  $0.19 \pm 0.4$   $\mu\text{A}$ ). This anodic control utilized environmental conditions mirroring the cathodic condition (no carbon added, oxygen provided, etc.) while altering the potential on the electrode to a level where a minimal reduction current occurs, therefore preventing cathodic electron flow. This control accounts for background heterotrophy and/or cellular energy obtained from storage products in this carbon-free system. One caveat is the difficulty in controlling for variation in the physiological responses to changes in potential, including possible increased carbon/electron equivalents added to this system from decaying cell biomass or hydrogen produced on the counterelectrode. Nonetheless, the ATP/(ADP plus ATP) ratio was significantly higher under cathodic conditions than under either control condition (Fig. 4). While we did not quantify AMP levels, the ATP/(ATP plus ADP) ratios also supported an increase in the energy charge state (26) of the cells under cathodic conditions.

Statistically significant cell loss was observed in open-circuit controls (Fig. S8), likely due to the lack of energy input required to maintain cell biomass on the electrode. Because of this, ATP levels fell below that assay detection limit. Unlike with the open-circuit controls, cell biomass does not statistically change throughout the course of the experiments when poised electrodes have been used ( $2.2 \times 10^7 \pm 5 \times 10^6$  and  $2.3 \times 10^7 \pm 1.2 \times 10^7$  cells per biofilm for cathodes and minimal anodes, respectively). The per-cell ATP values estimated in this work fall between  $0.13$  and  $0.68$  fmol of ATP

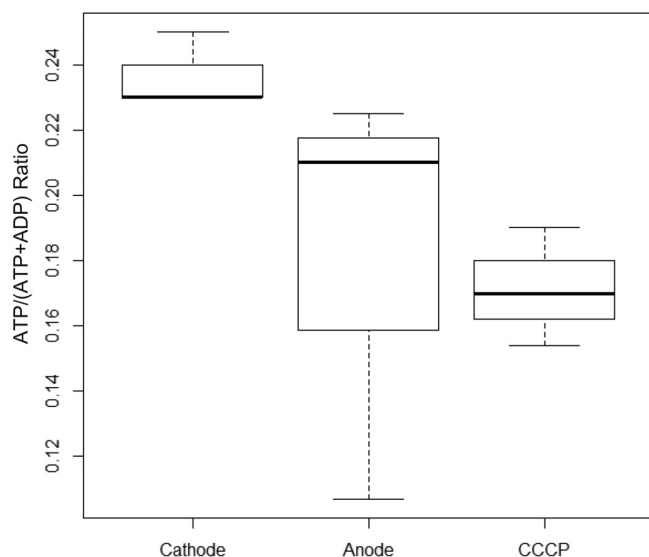


**FIG 4** Larger ATP pools were observed under cathodic conditions. ATP levels were normalized to those of combined ATP and ADP levels recovered from MR-1 biofilms maintained under poised electrode conditions ( $-303$  or  $197$  mV versus the voltage of the SHE) for 24 h. The conditions compared reflect cathodic-current generation with an electrode potential poised at  $-303$  mV (Cathode) ( $n = 9$ ), minimal anodic-current generation with an electrode potential of  $197$  mV (Anode) ( $n = 9$ ), and cathodic-current generation as described above with a 3-h CCCP treatment prior to ATP recovery (CCCP) ( $n = 9$ ). All treatments were performed under exogenous-carbon-free and aerobic environmental conditions. Box plot reflects the median mean (bold black lines), 1 standard deviation around the mean (box), and the data spread (dashed lines).

per cell ( $7.8 \times 10^7$  to  $4.1 \times 10^8$  ATP molecules per cell). Though cellular ATP levels can vary across microbes, as can growth rates (shown to range 6 orders of magnitude across taxa) (27), the per-cell ATP levels observed in this work were similar to those of environmentally sampled *Escherichia coli* cells (0.18 to 0.25 fmol per cell) (27, 28).

The observed difference in ATP/(ATP plus ADP) ratios between wild-type *S. oneidensis* MR-1 cathodic biofilms and *S. oneidensis* MR-1 cathodic biofilms treated for 3 h with CCCP (Fig. 4) supports the notion that *S. oneidensis* MR-1 generates a proton gradient during cathode oxidation, as ATP levels are lower in the presence of an uncoupler. While the differences observed between cathodic experiments with and without the uncoupler are small, they are significant on a per-cell basis, as they equate to a minimum difference of 4 million ATP molecules. These 4 million molecules, assuming a steady-state ATP concentration under cathodic conditions, represent the net consumption of ATP over a 3-h period (equaling the amount produced over the time frame of CCCP addition to maintain steady-state levels). However, this may capture only a small fraction of the per-cell ATP flux (the total ATP production over time accounts for losses due to consumption). The amount of current required to generate 4 million ATP molecules in a cell is 0.19 to 0.05 fA over a 3-h period (assuming 1 to 4 protons pumped per electron and 3.3 protons required per ATP). Though this is the lowest conservative estimate of ATP being generated in a 3-h period, these values represent 0.2 to 0.01% of the range of per-cell currents observed (50 to 100 fA) over this time frame. This estimate does not account for the total potential ATP turnover within cells and/or other sinks for PMF under these conditions, both of which might be significant given the unaccounted-for PMF. For example, depending on the degree of proton accumulation, this PMF might also aid in reverse electron flow (i.e., electron flow from the generally higher potential quinone pool to oxidized cellular electron carriers), resulting in the generation of cellular reducing equivalents (i.e., NADH) from the cathodic electron flow (model illustrated in Fig. 1B).

To directly test whether cathodic electron flow can be converted to cellular reducing power in the form of NAD(P)H and/or FMNH<sub>2</sub>, we used the bacterial luciferase enzyme,

inserted downstream of the *glmS* gene into a neutral site in the bacterial genome via transposition with the *lux* operon (*luxCDABE*) (29) as a real-time *in vivo* marker for the cellular redox pool. The Lux enzyme system performs a well-characterized cytoplasmic process that generates light using an oxygen molecule, reduced flavin mononucleotide (FMN<sub>H<sub>2</sub></sub>), and an activated (via NADPH and ATP) aldehyde functional group (30). Though there are multiple factors that influence light production, the cellular redox state (overall ratio of reduced to oxidized cellular electron carriers) has been shown to be proportional to the amount of light produced by the cell (31–33). In these experiments, expression of the *lux* operon is constitutively driven by the P1 promoter, resulting in consistent light production under aerobic growth conditions. The variation of enzyme levels, depending on the growth history of the cells, made it difficult to compare levels of light production quantitatively across different experiments where the energy investment in protein production varied. However, comparing across cell populations with similar growth histories and maintaining nonlimiting oxygen and aldehyde concentrations for the Lux reaction, we could correlate lactate concentration (which in turn affects respiration rate, electron flow, and the redox pool) to light production across normalized cell populations (Fig. S2). This provides support to the possibility of the Lux reaction yielding information about the cellular energy state, despite natural variation across populations.

Light production was limited for aldehyde under cathodic conditions (no exogenous carbon), as demonstrated by the rapid increase in light production when 0.002% decanal was provided (a modest initial increase likely due to aldehyde diffusion across the cell membrane), peaking 0.5 h after decanal addition (Fig. 5). Increased light production does not appear to be based on decanal conversion to reducing power, as no light was observed under the control conditions (minimal anodic current condition), and *S. oneidensis* MR-1 did not grow aerobically with decanal as the sole carbon source. Though it was difficult to compare light intensities across various experiments, the trend of increasing light production with increasing current consumption compared to levels in controls was consistently observed and was independent of the order of poised potential conditions (Fig. S3). We also noted that the magnitude of current generated was positively correlated with light production (Fig. S3). Given the variety of potential sources of reducing equivalents in *S. oneidensis* MR-1 (cellular storage products, endogenous cell decay, etc.), it is difficult to determine whether there is a direct link between cathodic electrons and the cellular reducing pool (total cellular electron carriers) from these data alone. However, the increase in the cellular reducing pool observed in *SO-lux* strains (strains in which the *lux* operon was inserted into the *S. oneidensis* MR-1 genome via transposition at a neutral site via a mini-Tn7-*luxCDABE-tp* cassette), along with the likelihood of PMF generation from the cathodic electron flow, supports the possibility that reverse electron flow operates in *S. oneidensis* MR-1 cells under cathodic conditions.

**Reverse electron flow enhances the cellular reducing pool in *S. oneidensis* MR-1.** Reverse electron flow involves utilizing a proton gradient to drive electrons from a higher potential state (i.e., quinone pool) to a lower potential state (i.e., NAD<sup>+</sup>) in the cellular electron transport chain (34, 35). Under conditions of reverse electron flow, generation of NADH can be inhibited by a protonophore uncoupler (36). To determine whether cathodic electron flow resulted in an enhanced redox pool through reverse electron flow, the protonophore uncoupler CCCP was used in combination with the *SO-lux* strain to determine whether collapse of the inner membrane proton gradient affected light generation via the luciferase enzyme, with light utilized as an intracellular marker for the cellular redox pool. Addition of CCCP to the *SO-lux* strain showed a marked decrease (by nearly an order of magnitude) in light production (Fig. 6A), though no statistically significant effect was observed on the current (Fig. S4). The inhibitory effects of CCCP on light production were mitigated by addition of lactate under otherwise-identical cathodic conditions (Fig. S5). It is difficult to distinguish between the effects of ATP and NAD(P)H in these *SO-lux* strain experiments, as both NAD(P)H and ATP are (i) required for the luciferase reaction, (ii) likely linked to proton motive



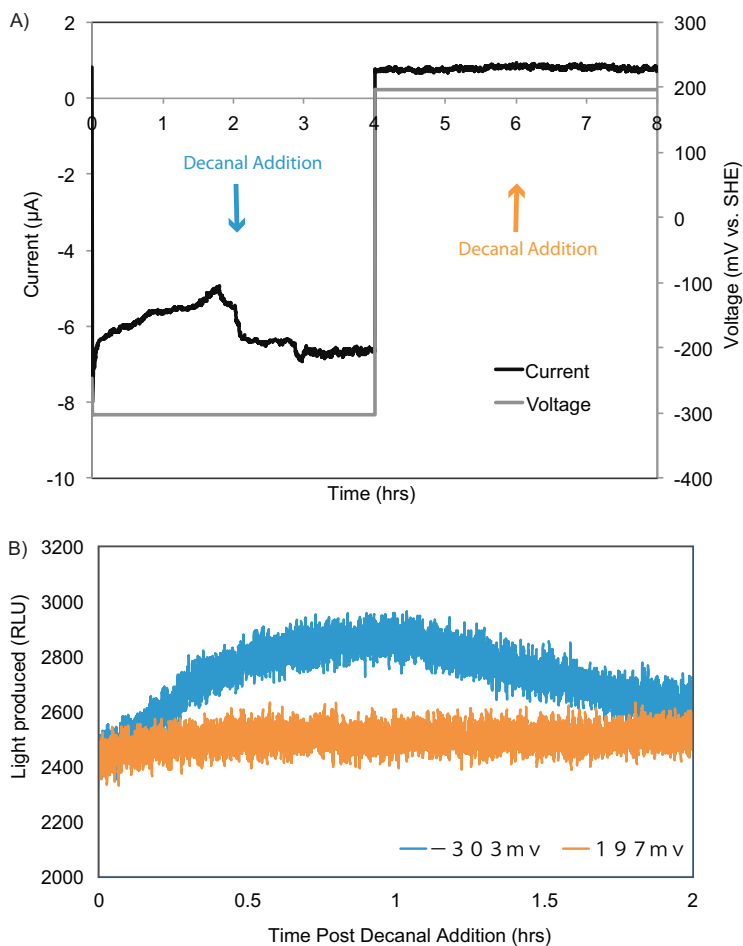


**FIG 5** Luciferase light production is significantly higher under cathodic conditions than under anodic conditions for the same biofilm. (A and B) Representative demonstrations (one of four) of the *SO-lux* mutant electrode biofilm current (A) and light production for an electrode poised at a cathodic-current-generating redox potential ( $-303$  mV versus the voltage of the SHE, 0 to 4 h) and then switched to a noncathodic redox potential ( $197$  mV the voltage of the SHE, 4 to 8 h), where minimal anodic current was observed (B). Decanal was added at a concentration of 0.002% at 2 h into each poised potential incubation (as indicated by the colored arrows). (B) Light production was quantified by a photon-multiplying tube and is presented in relative light units (RLU) for the 2-h period after decanal addition, which corresponds to the 2-h period following the blue and orange arrows shown in panel A.

force (either via reverse electron flow or ATPase activity) and are therefore affected by CCCP addition, and (iii) products of lactate metabolism (ATP via substrate-level phosphorylation and NADH via lactate dehydrogenase activity) independently of PMF, which might explain lactate mitigating the effects of CCCP. This makes it difficult to link the effects of CCCP to the reverse electron flow using these wild-type experiments alone. Because of this, *SO-lux* strains with various electron transport chain components deleted were also evaluated.

A similar decline in light production was observed with the  $bc_1$  complex mutant of *S. oneidensis* containing the *lux* operon ( $\Delta petABC-lux$  strain) when CCCP was added (Fig. 6B). The  $bc_1$  complex is not essential to the aerobic respiratory electron transport chain (37), as *S. oneidensis* MR-1 has multiple ETC routes to reduce oxygen (18, 38). However, the PetABC complex has the potential to maximize PMF generation under aerobic conditions (i.e., in the Q cycle versus the Q loop) (36). Additionally, the observed loss of light production upon CCCP addition suggests that PetABC is not involved in mediating electron flow to the cellular redox pool in *S. oneidensis* MR-1, as has been suggested for other organisms (39, 40). Unlike with other mutants, in the  $\Delta nuo-lux$  strain (complex I deletion in *S. oneidensis* is amended with *lux*), CCCP addition did not

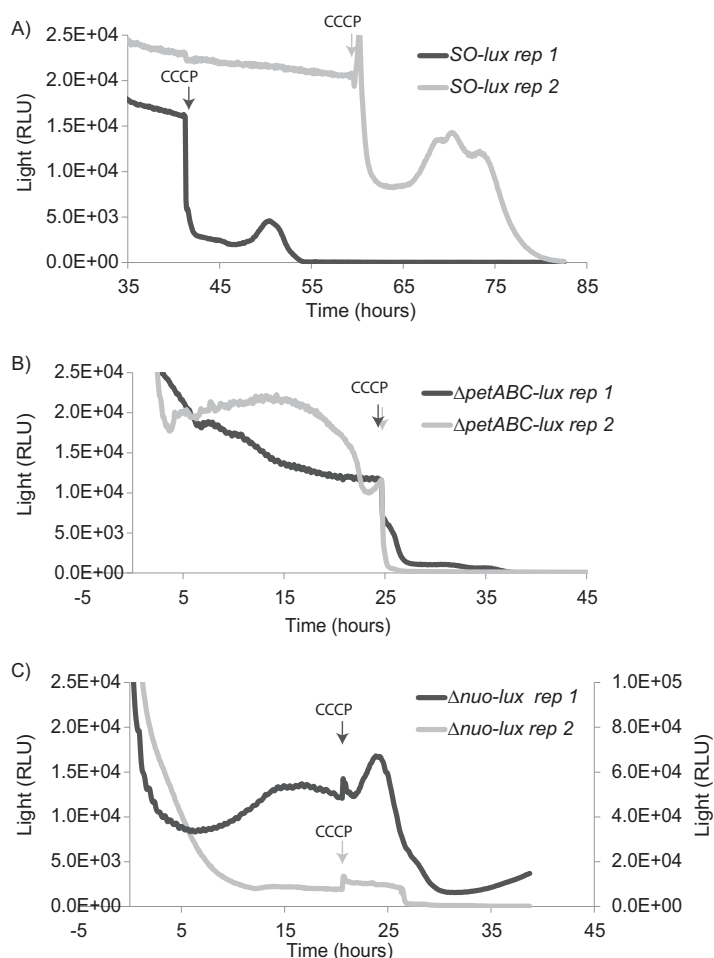


**FIG 6** Light production is inhibited by CCCP addition, unless the complex I gene is deleted. (A to C) Light was quantified in cathodic biofilms poised at  $-303$  mV (versus the voltage of the SHE) for two (of three) replicates (rep 1 and 2) of the following MR-1 strains amended with the *lux* operon: wild-type MR-1 (*SO-lux*) (A), the *bc<sub>1</sub>* complex mutant (*ΔpetABC-lux*) (B), and the complex I mutant (*Δnuo-lux* mutant) (C). After at least 20 h under cathodic conditions and at the time points indicated by arrows on each plot, the protonophore uncoupler CCCP was added to each reactor. Light was measured via a photon multiplier tube and is presented in relative light units (RLU). Plots depict the 45- to 50-h period around CCCP addition. Replicate 1 with the *Δnuo-lux* mutant demonstrated 2-fold-higher light intensities, and its results are therefore plotted on a larger light intensity scale (right axis in panel C).

result in a decline in light production within the first 15 min of addition (Fig. 6C). Complex I is a reversible proton-pumping NADH/ubiquinone-oxidoreductase (41, 42) that has been implicated in reverse electron flow in other organisms (34, 35, 43, 44). In the *Δnuo-lux* strain, steady light production was observed for a  $>5$ -h period until ultimately declining, consistent with the ultimate decline in cell health resulting from CCCP addition. The observation that, in the absence of complex I, PMF does not have the same effect on cellular light production implicates reverse electron flow in *S. oneidensis* MR-1. The most probable cause for this phenomenon in the *Δnuo-lux* strain compared to the wild type is the inability to couple PMF and NADH reduction, which would explain the lack of change in the cellular reducing pool (or light production) upon CCCP addition. This result could be recreated in the wild-type *SO-lux* strain when the complex I-specific inhibitor piericidin A was added to a cathodic biofilm. Piericidin A addition prevented the decrease in light production observed in the wild-type cells alone (Fig. S5). This further supports a role for complex I in generating reducing equivalents via a reverse electron flow under cathodic conditions in *S. oneidensis* MR-1.

CCCP also did not affect light production under the control condition where a minimal oxidizing potential was poised and a minimal anodic current was observed

(averages,  $23 \pm 1$  and  $34 \pm 3$  nA) (Fig. S5). Though it is difficult to exclude the possibility that ATP is involved in the effects on light production seen upon CCCP addition, in order for ATP levels to drive the results seen with the  $\Delta nuo-lux$  strain with piericidin A and the minimal-anodic-current controls, the standing ATP pools in these experiments would have to be significantly larger than in wild-type experiments. There is no obvious mechanism that would support this phenomenon (enhanced ATP pools) in all three scenarios. This supports the likelihood of reverse electron flow under cathodic conditions being the major driver of these observations, which from the cumulative luciferase experiments demonstrate dependence on (i) cathodic electron flow, (ii) an oxidized redox pool and/or electron donor-limited conditions, and (iii) the presence of a reversible proton-translocating NADH/ubiquinone oxidoreductase for reverse electron transport to occur.

**Cathode oxidation results from a reversal of multiple extracellular electron transport routes in *S. oneidensis* MR-1.** To assess the route of electron flow into cells under cathodic conditions, we utilized a set of gene deletion mutants of various extracellular electron transport pathways, as well as inner membrane electron transport chain mutants (Table 1; illustrated in Fig. 1). Of the mutants tested, the mutant deficient in all three of the terminal cytochrome oxidases ( $\Delta cox$ -all mutant) demonstrated the greatest percentage decrease in current consumption, though the individual cytochrome oxidase mutants displayed near wild-type cathodic-current levels (Table 1; Fig. S6). Deletion of all five outer membrane multiheme cytochromes ( $\Delta omc$ -all mutant) also significantly decreased current consumption; it was only slightly greater than that of the  $\Delta mtrC \Delta omcA$  double mutant (Table 1; Fig. S6). However, minimal cathodic currents were observed in the majority of other cytochrome mutants tested, including a variety of periplasmic electron carriers. Surprisingly, this included proteins like DmsE, a periplasmic decaheme cytochrome shown to be associated with dimethyl sulfoxide (DMSO) reduction (45). Some cathodic-current generation could be recovered when a copy of the *dmsE* gene behind the ribosomal binding site of *mtrA* was introduced into the  $\Delta dmsE$  mutant in *trans*. Coupled with the observation that other *dms* deletion mutants (*dmsB* and  $\Delta dms$ -all mutants) significantly decrease cathodic-current generation, there is the potential that multiple extracellular electron transport pathways run in parallel and/or cooperatively during cathode oxidation. It is difficult, however, to distinguish the hypothesis of parallel pathways of cathodic electron flow from the possibility of differential gene expression affecting cathodic-current generation among the various mutants.

Cyclic voltammetry (CV) was performed on all mutant strains utilized in these experiments. The only two mutants to demonstrate CV profiles for aerobic cathodic electron flow similar to that of the wild type (Fig. 7) were the  $\Delta fccA$  and  $\Delta ccoO$  mutants (data not shown). The other mutants tested showed a significantly decreased onset potential and/or magnitude of cathodic electron flow that was only slightly enhanced from those of controls (data not shown), consistent with the observed decrease in current generated during chronoamperometry experiments for these mutants. Interestingly, a 180- to 200-mV increase in onset potential was observed when we compared *S. oneidensis* MR-1 aerobic/oxygen-reducing cathodic biofilms and *S. oneidensis* MR-1 anaerobic/fumarate-reducing cathodic biofilms (Fig. 7). Under aerobic conditions, we observed a 0- to 20-mV cathodic-current onset potential versus that of the SHE, whereas under anaerobic conditions with fumarate, we observed an onset potential of  $-160$  to  $-180$  mV versus that of the SHE (Fig. 7); these match the corresponding potentials proposed for the outer membrane cytochromes with unbound and bound flavins, respectively (46). These observed redox potentials further support the role of outer membrane cytochromes in cathode oxidation, though it does not exclude the possible activities of other pathways with similar oxidation reduction potentials. In addition, these results also support the requirement for reverse electron flow to generate cellular reducing equivalents, such as NADH from  $NAD^+$ , given the 300 mV more negative redox potential observed between the midpoint potential of elec-

**TABLE 1** *Shewanella oneidensis* MR-1 strains used in this study

Strain	Gene deletion(s)	Reference or source <sup>a</sup>	Description	% reduction in normalized cathodic current compared to that of the wild type <sup>b</sup>
MR-1 wild type		55		
$\Delta mtrC \Delta omcA$ mutant	SO1778, SO1779	68*	Outer membrane decaheme cytochrome gene deletions	88.2 $\pm$ 6.7
$\Delta omc$ -all mutant	SO1778–SO1782, SO2931, SO1659	69*	Deletion of all outer membrane multiheme cytochrome gene homologs	95.7 $\pm$ 3.2
$\Delta cymA$ mutant	SO4591	68*	Tetraheme cytochrome <i>c</i> quinone oxidase gene deletion	85.2 $\pm$ 0.1
$\Delta PEC$ mutant	SO1777, SO1782, SO1427, SO4360, SO2277	65*	Deletion of genes for periplasmic electron carriers: MtrA, MrtD, DmsE, SO4360, CctA (small periplasmic tetraheme cytochrome)	82 $\pm$ 1.3
$\Delta mtrA$ mutant	SO1777	68*	Periplasmic decaheme cytochrome gene deletion	72.3 $\pm$ 4.5
$\Delta fccA$ mutant	SO0970	68	Fumarate reductase, periplasmic tetraheme flavochrome gene deletion	4.4 $\pm$ 11.2
$\Delta dmsE$ mutant	SO1427	68	Gene deletion of MtrA homolog involved in DMSO reduction	92.4 $\pm$ 0.3
$\Delta dmsE::p(mrtA_{rb})dmsE$ mutant <sup>c</sup>	SO1427	This work	<i>dmsE</i> gene deletion mutant containing the plasmid <i>dmsE</i> gene 38 bp upstream of the <i>mtrA</i> sequence in pBBR1MCS-2 (65)	57.6 $\pm$ 3.8
$\Delta dmsB$ mutant	SO1430	45*	Lacking the iron-sulfur cluster subunit of the Dms operon	93.5 $\pm$ 1.2
$\Delta dms$ -all mutant	SO1427–SO1432	This work	Lacking the DMSO reductase operon ( <i>dmsEFABGH</i> )	91.8 $\pm$ 0.3
$\Delta petABC$ mutant	SO0608–SO0610	This work	Lacking the cytochrome <i>bc</i> <sub>1</sub> complex genes	86.3 $\pm$ 1.8
$\Delta nuo$ mutant	SO1018 (partial), SO1019–SO1017	This work	Full-gene deletion of <i>nuoE</i> , a portion of <i>nuoF</i> (5') from the NADH-oxidizing N module, and partial deletion of <i>nuoC</i> and <i>nuoD</i> (3') from the iron sulfur-containing Q module	95.3 $\pm$ 4.4
$\Delta ccoO$ mutant	SO2363	68	Deletion of the gene for cytochrome <i>c</i> oxidase, <i>ccb</i> <sub>3</sub> type, subunit II	40.7 $\pm$ 2
$\Delta cox$ -all mutant	SO2361–SO2364, SO3285–SO3286, SO4606–SO4609	This work	Lacking all the terminal cytochrome <i>c</i> oxidase genes, including <i>ccb</i> <sub>3</sub> , <i>bd</i> (low oxygen concentration), and <i>aa</i> <sub>3</sub>	96.5 $\pm$ 1.2
<i>SO-lux</i> mutant		This work	Mini-Tn7- <i>lux(CDABE)</i> - <i>tp</i> cassette inserted into a neutral site downstream of the <i>glmS</i> gene (29) in the wild-type background	NC
$\Delta petABC$ - <i>lux</i> mutant	SO0608–SO0610	This work	Mini-Tn7- <i>lux(CDABE)</i> - <i>tp</i> cassette inserted downstream of the <i>glmS</i> gene (29) in the $\Delta petABC$ mutant background	NC
$\Delta nuo$ - <i>lux</i> mutant	SO1018 (partial), SO1019–SO1017	This work	Mini-Tn7- <i>lux(CDABE)</i> - <i>tp</i> cassette inserted downstream of the <i>glmS</i> gene (29) in the $\Delta nuo$ mutant background	NC

<sup>a</sup>An asterisk indicates that mutant complementation was performed in the indicated reference.

<sup>b</sup>Shown are the percentages of reduction in the normalized cathodic current observed (Fig. S6) in gene deletion mutants compared to the cathodic current of the wild type (values were not calculated [NC] for *lux* insertion mutants).

<sup>c</sup>Promoter of gene altered to contain the ribosomal binding (*rb*) site of the *mrtA* gene (SO1777).

tron uptake in *Shewanella* (0 to 20 mV versus the voltage of the SHE) and NADH ( $E^{\circ}$  [pH 7] = -320 mV versus the voltage of the SHE) (47).

**Implications for cathode oxidation in minimizing cellular decay.** As expected, cell growth was not observed over a 5-day period with cathodic conditions imposed (Fig. S7A). However, cell decay (loss of cell biomass through death and lysis) was also not observed under cathodic conditions. Open-circuit conditions demonstrated a statistically significant loss in surface-attached cell biomass over the same experimental period (an approximately 17% cell loss per day) (Fig. S7). This survival stands in sharp contrast to the cellular decay rate of planktonic cells under comparable conditions (with the identical medium and a similar starting optical density [OD]), where a 48% loss of biomass is expected over the same period (Fig. S7). While it is difficult to distinguish cell detachment from cell decay under biofilm conditions, over a 5-day period, the loss of cell biomass observed under the minimal-anodic-current condition is consistent with the amount of cell loss observed under open-circuit conditions (an ~4-day half-life) though not statistically significant within a 24-h period (Fig. S7). These observations add

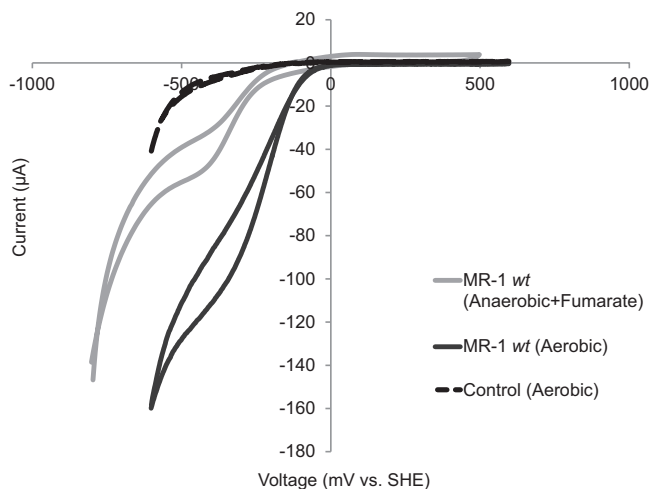


**FIG 7** Cathodic electron uptake in MR-1 cells shifts to more positive potentials under oxic conditions than under anoxic conditions. Shown are cyclic voltammograms taken for an MR-1 cathodic biofilm poised at  $-303$  mV (versus the voltage of the SHE) incubated under aerobic conditions with oxygen as a terminal electron acceptor and under anaerobic conditions with fumarate as a terminal electron acceptor (17). CV results of one of three experiments are also shown for a cell-free abiotic control under aerobic conditions (dashed line). Scans were run at  $5$  mV/s under aerobic conditions and  $10$  mV/s under anaerobic conditions. *wt*, wild type.

further support to the capacity for cellular energy acquisition under cathode-oxidizing conditions and imply that this energy may be harnessed to provide cell maintenance to stave off cell death and decay and/or maintain cellular attachment in a biofilm.

## DISCUSSION

This report describes evidence of cellular energy acquisition in *S. oneidensis* MR-1 from cathode oxidation coupled to oxygen reduction. The periplasm and outer membrane of *S. oneidensis* MR-1 are enriched in redox-active cytochromes, raising the possibility that electrons from an exterior cathode are routed along this redox network to a terminal oxidant in a biocatalytic process, rather than that they interact with inner membrane components that would, via generation of an electrochemical gradient, allow cells to acquire energy. This work combines a variety of genetic, biochemical, and electrochemical investigations to understand both the interactions of cathodic electrons with cellular components and the physiological consequences of these interactions.

Though a model for electron flow was developed for *S. oneidensis* MR-1 anaerobic-cathode oxidation using fumarate as an electron acceptor (16, 17), much less was known about electron flow under cathodic conditions with oxygen used as a terminal electron acceptor. Analysis via cyclic voltammetry suggests a distinct redox potential difference in the routes of entry from *S. oneidensis* MR-1 cells under aerobic conditions and anaerobic conditions (Fig. 7). It should be noted that this redox potential is higher than the standard redox potentials for both NAD(P)H and hydrogen at pH 7. Our results are consistent with cathodic activity under aerobic conditions being mediated by a *c*-type cytochrome without a bound flavin, as the redox potentials that we observed are in line with those reported for Mtr proteins lacking flavins (10, 46). This result is consistent with the proposed model that flavin binding is prevented by a disulfide bond formed under aerobic conditions in MtrC, OmcA, and MtrF (48).

While these outer membrane multiheme cytochromes likely play an essential role in cathode oxidation, our data suggest that the canonical *S. oneidensis* MR-1 cytochromes (MtrC and homologs) are not the only cytochromes important for cathodic function (Table 1). Although the use of gene deletion mutants suggests several possible pathways, the degree of decrease in cathode-oxidizing activity in nonredundant or parallel pathways suggest that either (i) the architecture of the cytochrome network is in some

way cooperative and/or plays an important functional role in the rate of cathodic electron flow or (ii) differential levels of gene expression across the deletion mutants tested are responsible for the altered cathode oxidation activity. Because of this, the explicit route(s) of electron flow from the cathode remain unclear; however, the interaction of cathodic electrons with the cellular electron transport chain, specifically in protein components that interact with protons (i.e., the  $bc_1$  complex and complex I), is supported by this work (Table 1). Combined with evidence from electron transport chain inhibitor studies (Fig. 2 and 3) and ATP quantification (Fig. 4), these data strongly suggest the generation of proton motive force and subsequent utilization for cellular processes under aerobic and cathodic conditions.

The route of electron flow determined under anaerobic conditions also involves reversal of the Mtr pathway, but energy acquisition under these conditions was not determined (16). The relatively small redox potential difference between an electron in the Mtr pathway and fumarate, as well as the potential for direct interactions between these proteins (8), makes it unlikely that these redox couples drive proton pumping; the standard redox potentials are reported to be lower than those of known coupling sites which utilize  $>180$  mV to translocate a proton (36). Conversely, the energetics for aerobic-cathode conditions, owing to the greater reduction potential of oxygen, is more thermodynamically favorable, which likely results in different physiological consequences between aerobic- and anaerobic-cathode processes, namely, the ability of electrons to enter the aerobic electron transport chain.

The magnitude of PMF accumulation under aerobic-cathode conditions is likely not only linked to the production of ATP. This work presents evidence for the generation of cellular reducing equivalents [i.e., NAD(P)H and FMN] during cathodic conditions (Fig. 5). Experiments utilizing a luciferase bioassay, protonophore uncouplers, and mutants in the aerobic cellular electron transport chain suggest that reverse electron flow (the reduction of lower potential electron carriers utilizing PMF as an energetic driving force) can be utilized by *S. oneidensis* MR-1 to generate reduced cytoplasmic electron carriers under cathodic conditions (Fig. 6). Light production via luciferase has been shown to be directly dependent on FMN<sub>2</sub> levels and indirectly on NAD(P)H levels and ATP (30). NAD(P)H, in particular, is required for the activation of the aldehyde moiety (LuxCE) (30) and can be used to regenerate FMN<sub>2</sub> that is used directly, a process catalyzed by endogenous cellular enzymes (31, 49–51). While the luciferase reaction is not a quantitative marker of NAD(P)H levels specifically, the effect of CCCP on light production under a variety of scenarios supports the connectivity between cellular reducing equivalents and PMF via reverse electron flow.

The main observations that led to this hypothesis are that under NADH-limiting conditions (i.e., electron donor limitation), in the presence of NADH-ubiquinone oxidoreductase complex I (a reversible enzyme that has been shown to generate NADH using PMF), and with cathodic electron flow, the addition of a protonophore uncoupler results in a rapid decrease (within 15 min) in light production, likely reflecting the loss of NADH generation from reverse electron flow. Subsequently, the lack of complex I, addition of a carbon source, or lack of cathodic electron flow does not result in a similar collapse in the luciferase reaction. Reverse electron flow of electrons from a cathode to NADH mediated by complex I in the presence of predominantly oxidized cellular electron carriers is the model that accounts for these experimental observations. Other hypotheses may account for some of these observations. The collapse in ATP production that occurs due to the loss of PMF might also inhibit the luciferase reaction; however, it is unclear how or why ATP collapse from CCCP would differentially affect the  $\Delta nuo$ -lux strain and the  $\Delta petABC$ -lux and  $SO$ -lux strains. Additionally, measurable ATP was observed in the wild-type strain after 3 h of CCCP addition (Fig. 4). Alternatively, under predominantly heterotrophic conditions, uncoupler addition can result in high rates of NADH oxidation due to the amelioration of PMF. This can, in turn, inhibit proton-translocating electron transport chain components. If this mechanism occurs, the collapse of light production upon CCCP addition would likely have been observed in both the lactate-amended experiments and the complex I deletion experiments.



Notably, MR-1 has alternate and non-proton-pumping NADH/quinone-oxidoreductases (i.e., *ndh*) (52, 53), which allows for NADH oxidation in the  $\Delta nuo$  background.

Reverse electron flow, as has been described in chemolithoautotrophs, utilizes high-potential electron donors as a sole electron source (34, 35, 54). Implicit for cellular biosynthesis and/or carbon fixation is the conversion of NADH to a variety of cellular electron carriers utilized in anabolism, most commonly NADPH (36). These reducing equivalents are critical for biosynthesis, and the observation of enhanced maintenance of cell biomass (or slower death) under cathodic conditions further supports the idea that reducing equivalents are generated from cathodic electrons. Though we provide evidence for the generation of cellular energy carriers [i.e., ATP and NAD(P)H] in this system, there was no evidence of cell growth/division under these conditions. No growth was expected given that these experiments were performed in a system that lacked exogenous carbon inputs and several growth factors (i.e., vitamins and amino acids) that could provide carbon (55), and the *S. oneidensis* MR-1 genome contains no known complete carbon fixation pathway (38). However, the energy conserved in the form of ATP and cellular reducing power might plausibly support cell maintenance under cathodic conditions. As cathode biomass was maintained past the expected cell decay rates, it seems likely that the energy acquired is being invested in cellular upkeep. This is further supported by previous observations of *S. oneidensis* MR-1 that demonstrated that this organism requires energy in order to maintain cell surface attachment (56) and that such energy acquired under cathodic conditions might also be devoted to maintaining attachment. These observations support the proposal that MR-1 cells acquire energy for cellular processes under the studied cathodic conditions, energy that prolongs cell survival and/or allows maintenance of cell attachment.

The ability of *S. oneidensis* MR-1 to conserve energy under aerobic-cathode-oxidizing conditions may have important implications for the utility of this organism for microbe-electrode applications. The specifics of how electrons enter the cell and how this is coupled to a terminal electron acceptor affect cellular energy levels, the potential for growth, cell maintenance, and the overall process rates and long-term activities of these reactions. The environmental implications of these observations are more difficult to assess. In essence, are there environmental conditions under which *S. oneidensis* MR-1 can capitalize on the reversibility of the extracellular electron transport systems for acquiring energy for cell maintenance? *Shewanella* is an environmentally ubiquitous genus that is often found in redox transition zones or complex sediments (57). It is likely that this organism is commonly faced with shifts from anaerobic to aerobic conditions and/or carbon limitation. Though it appears to be a rate-adapted organism under carbon-replete anaerobic conditions (trading reaction rates for energetic efficiency), it may possess mechanisms for persistence in variable environments that are not presently well understood. Our results suggest the possibility that *S. oneidensis* MR-1, under carbon-limiting conditions in the presence of oxygen, capitalizes on solid-phase electron donors (e.g., sulfides and reduced iron species, possibly ones generated previously in the absence of oxygen) as electron sources for non-growth-linked energy acquisition. This may highlight an important ecologic advantage to such a reversible extracellular electron transport pathway, as has been suggested for iron cycling between iron-reducing and iron-oxidizing microbes (58). This work may also have implications for understanding electron uptake in organisms that can oxidize insoluble substrates (39, 58, 59), especially in the context of subsurface microbiology, as oxic, carbon-limited, and iron-rich (i.e., basalt) sediments are not uncommon in the deep sea (60, 61). Subsurface ecosystems often support orders of magnitude more microbes than should be allowable based on current energetic models and using the available organic carbon content (62). It has been postulated that lithotrophic interactions and especially lithoautotrophs might be part of this puzzle; however, when growth rates have been calculated, they are remarkably low (63). A non-growth-linked lithotrophic reaction might be a mechanism of potentially sustaining or slowing cell death and decay for subsurface microbes.

## MATERIALS AND METHODS

**Bacterial strains.** The bacterial strains used in this study are listed in Table 1. In the *SO-lux* strain constructed for this work, the *lux* operon was inserted into the *S. oneidensis* MR-1 genome via transposition at a neutral site via a mini-Tn7-*luxCDABE-tp* cassette (29), carrying both the *luxCDABE* operon behind the broad-host-range constitutive gamma-proteobacterial promoter P1 (derived from a dihydrofolate reductase gene [64]) and the gene for trimethoprim resistance. A transposon-containing plasmid was transferred to *S. oneidensis* MR-1 via conjugation from *E. coli* (WMB026 cells), along with the PTNS3 plasmid, encoding a transposase, in the WMB026 strain. Viable *lux* mutant strains were isolated on LB media with trimethoprim (200 mg/liter) and screened for bioluminescence.

The in-frame gene deletion mutants utilized in this work were constructed and validated as described previously (65). In brief, primers were designed (listed in Table S1 in the supplemental material) to amplify the flanking regions of the gene targeted for deletion. These amplicons were then ligated into a suicide vector. After vector transfer into *S. oneidensis* MR-1, strains were screened for double recombinants as described previously (66).

**Cathodic culturing conditions.** Prior to electrochemical experiments, *S. oneidensis* MR-1 was grown in a batch at 30°C in standard media previously described, including Luria broth (LB) and a defined medium containing 10 mM lactate as the predominant carbon source (DM-lactate) (17). Conditioning of electrodes for chronoamperometry experiments was performed as described previously (17). In brief, DM-lactate-grown *S. oneidensis* MR-1 cells were added to electrochemical cells at an OD at 600 nm of 0.25 in fresh medium with 10 mM lactate. To induce cell attachment to electrodes, the working electrodes were poised at 397 mV versus the voltage of the SHE, while the reactors were purged with nitrogen to maintain anaerobic conditions. After 20 to 30 h of incubation, planktonic cells were removed from the reactors along with remaining medium. The attached cells were rinsed three times in carbon-free DM (CF-DM). Carbon-free DM lacked not only lactate but also the yeast extract added to traditional DM. The culture medium used in electrochemical experiments also lacked both trace metal and vitamin amendments for cathode experiments, as these can interact abiotically with electrodes. Unless otherwise indicated, cathodic conditions were applied to rinsed attached electrode biofilms in CF-DM by poisoning a working electrode potential of -303 mV versus that of the SHE and while reactors were being bubbled with room air at a continuous and constant rate (5 to 10 ml/min).

The following electron transport chain inhibitors were added to cathode experiments at the indicated concentrations: 5 mM potassium cyanide, 20 μM antimycin A, and 5 nM piericidin A. Various antibiotics, ampicillin (100 μg/ml), kanamycin (100 μg/ml), and trimethoprim (100 μg/ml), were used for cloning and selection marker purposes. The protonophore uncoupler CCCP was added at concentrations of 20 to 40 μM. During Lux cathode experiments, the only alteration to the aforementioned protocol was the addition of decanal to a final concentration of 0.002% to the electrochemical cells at the time points indicated by arrows in the figures. To ensure that no deleterious effects of solvents on *S. oneidensis* MR-1 cells occurred, we determined the growth curves of the *SO-lux* strain of *S. oneidensis* MR-1 amended with the highest concentration of DMSO used (0.05%, for the addition of RSG), as well as 0.002% decanal, and compared them to normal aerobic growth in DM-lactate (Fig. S8).

**Electrochemical conditions.** The electrochemical cell used for these experiments was described previously (67) and was constructed in-house. In brief, each reactor comprised a working electrode constructed from ITO-coated glass (SPD Laboratory, Inc., Hamamatsu Japan), a counterelectrode of platinum wire, and a reference electrode of Ag-AgCl in a 3 M KCl solution (constructed in our lab). The main reactor type maintained a liquid volume of 10 to 12 ml to an electrode surface area of 3.75 cm<sup>2</sup>. Electrochemical cells were designed for use with purchased ITO-plated glass coverslips (SPI, Westchester, PA) that had a 3.61-cm<sup>2</sup> surface area to an 8-ml volume.

Experiments were performed using controlled voltage conditions and by measuring current production/consumption (i.e., chronoamperometry) through a potentiostat. The majority of chronoamperometry experiments were performed using eDAQ, quad channel potentiostats, and the corresponding eChart software (eDAQ Inc., Colorado Springs, CO); however, Lux chronoamperometry experiments were run on a Gamry 600 potentiostat using Framework software (Gamry, Warminster, PA) or a VMP3 potentiostat (BioLogic Company, France) using the parameters listed in the corresponding figure legends. Cyclic voltammetry was also performed using the Gamry 600 or the VMP3 potentiostat using the parameters listed in the corresponding figure legends.

**Fluorescence microscopy.** Electrode biofilms were visualized using an inverted microscope equipped with UV fluorescence detection. Cells were visualized using the lipid stain FM 4-64FX (Molecular Probes, Life Technologies, Inc.) at concentrations specified by the manufacturer. RedoxSensor Green (RSG) (Molecular Probes, Life Technologies, Inc.) studies were performed by adding approximately a 10 μM concentration of RSG in addition to lipid stain. Changes in fluorescence activity were monitored over time via microscopy. In brief, biofilm images were taken every 5 min over a period of 6 to 10 h, depending on the experiment. Fluorescence intensities between control (open-circuit), cathodic (applied reduced voltage), and inhibitor addition conditions were compared using approximately 80 images from each experimental state (including six different time points taken over a 30-min period). Cellular fluorescence intensities were compared for cells in each image using custom scripts in MatLab (codes are available upon request).

**ATP, ADP, and protein quantification.** Electrode biofilms were boiled for 10 min in nanopure water to release cellular ATP and ADP directly from electrode-attached cells. For protein recovery from electrode biofilms, samples were treated similarly, with the exception that 10 mM NaOH was added and samples were heated for at least 1 h at >85°C. Quantification of ATP and ADP was performed using the ATP/ADP ratio assay kit (Sigma-Aldrich Co.) according to the manufacturer's specification (standard

curves for ATP and ADP are provided in Fig. S9). Protein quantification was performed using the NanoOrange protein quantification kit (Molecular Probes, Life Technologies, Inc.) per the manufacturer's specifications. Both luminescence and fluorescence were quantified on a BioTek (Winooski, VT) Synergy H4 microplate reader available through the USC Nanobiophysics core facility (<http://dornsife.usc.edu/nanobiophysicore/>).

**Quantification of *in vivo* luciferase activity.** Light emissions from an electrode biofilm were detected across an ITO-coated glass electrode using a photon multiplier tube and associated software (Photon Systems Inc., CA). Uncoupler experiments were performed using either the above-named systems or a Gene Light 55 GL-100A luminometer (Microtec, Japan). All experiments were conducted in a dark box to minimize light contamination.

Light emissions for cells grown under various lactate concentrations were quantified in the same reactor setups; however, the ITO-coated glass was replaced with a glass microscope slide (Fig. S2). For these experiments, an LB-grown *SO-lux* strain was diluted into a DM amended with 7 mM lactate. After ~12 h of growth, cells were rinsed and resuspended at an OD at 600 nm of 0.2 in media with various lactate concentrations (7, 0.7, and >0.07 mM lactate). Light production was measured after density normalization and averaged over a 20-min period.

**Statistical methods.** All experiments were performed in biological replicates (three experiments were carried out unless specified otherwise). Statistical analyses were performed using R and/or Excel. In experiments where quantitative comparisons were made, data were normalized to cell biomass using either protein content (in the case of current comparisons for mutants) or the total nucleotide pool (in the case of ATP values). In most cases, the cell populations for each experiment were constrained by the surface area of the electrode (380 mm<sup>2</sup>) and by ensuring surface attachment and planktonic cell removal through repeated washings. Manual cell counts were performed in ImageJ for time zero and time final biofilms for each experiment to ensure that population sizes remained consistent (a 20 to 25% standard deviation from the mean value measured for single populations). Twenty images from each biofilm (accounting for 0.1 mm<sup>2</sup>) demonstrated a normal sample distribution around the mean. Results of representative experiments and mean values and standard deviations of biological replicates are reported in the figure legends or in the text.

## SUPPLEMENTAL MATERIAL

Supplemental material for this article may be found at <https://doi.org/10.1128/mBio.02203-17>.

**FIG S1**, EPS file, 1.7 MB.

**FIG S2**, EPS file, 1.3 MB.

**FIG S3**, EPS file, 2.5 MB.

**FIG S4**, EPS file, 10.6 MB.

**FIG S5**, EPS file, 24.9 MB.

**FIG S6**, EPS file, 1.2 MB.

**FIG S7**, EPS file, 2.4 MB.

**FIG S8**, EPS file, 1.1 MB.

**FIG S9**, EPS file, 1.3 MB.

**TABLE S1**, DOCX file, 0.01 MB.

## ACKNOWLEDGMENTS

We express our gratitude to Joanna B. Goldberg for supplying us with Lux plasmids from her 2013 study (29). Thanks go to Lina Bird for supplying the bacterial strain used for conjugation experiments, BW29427. We also acknowledge Alfred Spormann for editorial comments and suggestions on the manuscript.

Annette Rowe was funded primarily by a Center for Dark Energy Biosphere Investigations (C-DEBI) postdoctoral fellowship, followed by a NASA Astrobiology Institute (NAI) postdoctoral fellowship as part as the NAI Life underground team. Part of this work was performed during a JSPS fellowship by Annette Rowe (grant NNA13AA92A) with Kazuhito Hahimoto at Tokyo University, whom we sincerely thank for use of lab equipment. Work in the Nealson lab was funded by the Airforce Office of Scientific Research (grant GA9550-06-01-0292). Work in the El-Naggar laboratory was supported by an Innovation Fund Denmark Electrogas project (which partially supported Annette Rowe), and by the Division of Chemical Sciences, Geosciences, and Biosciences, Office of Basic Energy Sciences of the U.S. Department of Energy through grant DE-FG02-13ER16415. Abhiney Jain and Jeffrey Gralnick were supported by the Office of Naval Research (grant N000141310552). NASA funding for Annette Rowe, Kenneth Nealson, and Mohamed El-Naggar was provided by award number NNA13AA92A.

## REFERENCES

- Rabaey K, Rodríguez J, Blackall LL, Keller J, Gross P, Batstone D, Verstraete W, Nealon KH. 2007. Microbial ecology meets electrochemistry: electricity-driven and driving communities. *ISME J* 1:9–18. <https://doi.org/10.1038/ismej.2007.4>.
- Logan BE. 2009. Exoelectrogenic bacteria that power microbial fuel cells. *Nat Rev Microbiol* 7:375–381. <https://doi.org/10.1038/nrmicro2113>.
- Nealson KH, Rowe AR. 2016. Electromicrobiology: realities, grand challenges, goals and predictions. *Microb Biotechnol* 9:595–600. <https://doi.org/10.1111/1751-7915.12400>.
- Rabaey K, Rozendal RA. 2010. Microbial electrosynthesis—revisiting the electrical route for microbial production. *Nat Rev Microbiol* 8:706–716. <https://doi.org/10.1038/nrmicro2422>.
- Myers CR, Myers JM. 1997. Cloning and sequence of *cymA*, a gene encoding a tetraheme cytochrome *c* required for reduction of iron(III), fumarate, and nitrate by *Shewanella putrefaciens* MR-1. *J Bacteriol* 179:1143–1152. <https://doi.org/10.1128/jb.179.4.1143-1152.1997>.
- Marritt SJ, McMillan DGG, Shi L, Fredrickson JK, Zachara JM, Richardson DJ, Jeuken LJC, Butt JN. 2012. The roles of CymA in support of the respiratory flexibility of *Shewanella oneidensis* MR-1. *Biochem Soc Trans* 40:1217–1221. <https://doi.org/10.1042/BST20120150>.
- McMillan DGG, Marritt SJ, Butt JN, Jeuken LJC. 2012. Menaquinone-7 is specific cofactor in tetraheme quinol dehydrogenase CymA. *J Biol Chem* 287:14215–14225. <https://doi.org/10.1074/jbc.M112.348813>.
- McMillan DGG, Marritt SJ, Firer-Sherwood MA, Shi L, Richardson DJ, Evans SD, Elliott SJ, Butt JN, Jeuken LJC. 2013. Protein-protein interaction regulates the direction of catalysis and electron transfer in a redox enzyme complex. *J Am Chem Soc* 135:10550–10556. <https://doi.org/10.1021/ja405072z>.
- Sturm G, Richter K, Doetsch A, Heide H, Louro RO, Gescher J. 2015. A dynamic periplasmic electron transfer network enables respiratory flexibility beyond a thermodynamic regulatory regime. *ISME J* 9:1802–1811. <https://doi.org/10.1038/ismej.2014.264>.
- Hartshorne RS, Reardon CL, Ross D, Nuester J, Clarke TA, Gates AJ, Mills PC, Fredrickson JK, Zachara JM, Shi L, Beliaev AS, Marshall MJ, Tien M, Brantley S, Butt JN, Richardson DJ. 2009. Characterization of an electron conduit between bacteria and the extracellular environment. *Proc Natl Acad Sci U S A* 106:22169–22174. <https://doi.org/10.1073/pnas.0900086106>.
- Richardson DJ, Butt JN, Fredrickson JK, Zachara JM, Shi L, Edwards MJ, White G, Baiden N, Gates AJ, Marritt SJ, Clarke TA. 2012. The “porin-cytochrome” model for microbe-to-mineral electron transfer. *Mol Microbiol* 85:201–212. <https://doi.org/10.1111/j.1365-2958.2012.08088.x>.
- Hsu L, Masuda SA, Nealson KH, Pirbazari M. 2012. Evaluation of microbial fuel cell *Shewanella* biocathodes for treatment of chromate contamination. *RSC Adv* 2:5844. <https://doi.org/10.1039/c2ra20478a>.
- Rosenbaum M, Aulenta F, Villano M, Angenent LT. 2011. Cathodes as electron donors for microbial metabolism: which extracellular electron transfer mechanisms are involved? *Bioresour Technol* 102:324–333. <https://doi.org/10.1016/j.biortech.2010.07.008>.
- Rabaey K, Read ST, Clauwaert P, Freguia S, Bond PL, Blackall LL, Keller J. 2008. Cathodic oxygen reduction catalyzed by bacteria in microbial fuel cells. *ISME J* 2:519–527. <https://doi.org/10.1038/ismej.2008.1>.
- Bond DR, Lovley DR. 2003. Electricity production by *Geobacter sulfurreducens* attached to electrodes. *Appl Environ Microbiol* 69:1548–1555. <https://doi.org/10.1128/AEM.69.3.1548-1555.2003>.
- Ross DE, Flynn JM, Baron DB, Gralnick JA, Bond DR. 2011. Towards electrosynthesis in *Shewanella*: energetics of reversing the mtr pathway for reductive metabolism. *PLoS One* 6:e16649. <https://doi.org/10.1371/journal.pone.0016649>.
- Okamoto A, Hashimoto K, Nealson KH. 2014. Flavin redox bifurcation as a mechanism for controlling the direction of electron flow during extracellular electron transfer. *Angew Chem Int Ed Engl* 53:10988–10991. <https://doi.org/10.1002/anie.201407004>.
- Zhou G, Yin J, Chen H, Hua Y, Sun L, Gao H. 2013. Combined effect of loss of the *caa3* oxidase and Crp regulation drives *Shewanella* to thrive in redox-stratified environments. *ISME J* 7:1752–1763. <https://doi.org/10.1038/ismej.2013.62>.
- Meshulam-Simon G, Behrens S, Choo AD, Spormann AM. 2007. Hydrogen metabolism in *Shewanella oneidensis* MR-1. *Appl Environ Microbiol* 73:1153–1165. <https://doi.org/10.1128/AEM.01588-06>.
- Liu C, Gorby YA, Zachara JM, Fredrickson JK, Brown CF. 2002. Reduction kinetics of Fe(III), Co(III), U(VI), Cr(VI), and Tc(VII) in cultures of dissimilatory metal-reducing bacteria. *Biotechnol Bioeng* 80:637–649. <https://doi.org/10.1002/bit.10430>.
- Pirbadian S, Barchinger SE, Leung KM, Byun HS, Jangir Y, Bouhenni RA, Reed SB, Romine MF, Saffarini DA, Shi L, Gorby YA, Golbeck JH, El-Naggar MY. 2014. *Shewanella oneidensis* MR-1 nanowires are outer membrane and periplasmic extensions of the extracellular electron transport components. *Proc Natl Acad Sci U S A* 111:12883–12888. <https://doi.org/10.1073/pnas.1410551111>.
- Kalyuzhnaya MG, Zabinsky R, Bowerman S, Baker DR, Lidstrom ME, Chistoserdova L. 2006. Fluorescence in situ hybridization-flow cytometry-cell sorting-based method for separation and enrichment of type I and type II methanotroph populations. *Appl Environ Microbiol* 72:4293–4301. <https://doi.org/10.1128/AEM.00161-06>.
- Franks AE, Nevin KP, Glaven RH, Lovley DR. 2010. Microtoming coupled to microarray analysis to evaluate the spatial metabolic status of *Geobacter sulfurreducens* biofilms. *ISME J* 4:509–519. <https://doi.org/10.1038/ismej.2009.137>.
- Thöny-Meyer L. 1997. Biogenesis of respiratory cytochromes in bacteria. *Microbiol Mol Biol Rev* 61:337–376.
- Singer TP. 1979. Biomembranes, part F. Bioenergetics: oxidative phosphorylation. *Methods Enzymol* 1979.
- Karl DM. 1980. Cellular nucleotide measurements and applications in microbial ecology. *Microbiol Rev* 44:739–796.
- Shama G, Malik DJ. 2013. The uses and abuses of rapid bioluminescence-based ATP assays. *Int J Hyg Environ Health* 216:115–125. <https://doi.org/10.1016/j.ijheh.2012.03.009>.
- Venkateswaran K, Hattori N, La Duc MT, Kern R. 2003. ATP as a biomarker of viable microorganisms in clean-room facilities. *J Microbiol Methods* 52:367–377. [https://doi.org/10.1016/S0167-7012\(02\)00192-6](https://doi.org/10.1016/S0167-7012(02)00192-6).
- Damron FH, McKenney ES, Barbier M, Liechti GW, Schweizer HP, Goldberg JB. 2013. Construction of mobilizable mini-Tn7 vectors for bioluminescent detection of gram-negative bacteria and single-copy promoter *lux* reporter analysis. *Appl Environ Microbiol* 79:4149–4153. <https://doi.org/10.1128/AEM.00640-13>.
- Meighen EA, Dunlap PV. 1993. Physiological, biochemical and genetic control of bacterial bioluminescence. *Adv Microb Physiol* 34:1–67. [https://doi.org/10.1016/S0065-2911\(08\)60027-2](https://doi.org/10.1016/S0065-2911(08)60027-2).
- Galluzzi L, Karp M. 2007. Intracellular redox equilibrium and growth phase affect the performance of luciferase-based biosensors. *J Biotechnol* 127:188–198. <https://doi.org/10.1016/j.jbiotec.2006.06.019>.
- Koga K, Harada T, Shimizu H, Tanaka K. 2005. Bacterial luciferase activity and the intracellular redox pool in *Escherichia coli*. *Mol Genet Genomics* 274:180–188. <https://doi.org/10.1007/s00438-005-0008-5>.
- Shimada T, Tanaka K. 2016. Use of a bacterial luciferase monitoring system to estimate real-time dynamics of intracellular metabolism in *Escherichia coli*. *Appl Environ Microbiol* 82:5960–5968. <https://doi.org/10.1128/AEM.01400-16>.
- Kiesow LA. 1967. Energy-linked reactions in chemoautotrophic organisms. *Curr Topics Bioenerg* 2:195–233.
- Peck HDJ. 1968. Energy-coupling mechanisms in chemolithotrophic bacteria. *Annu Rev Microbiol* 22:489–518. <https://doi.org/10.1146/annurev.mi.22.100168.002421>.
- White D, Drummond J, Fuqua C. 2012. The physiology and biochemistry of prokaryotes, 4th ed. Oxford University Press, Oxford, United Kingdom.
- Brutinel ED, Gralnick JA. 2012. Anomalies of the anaerobic tricarboxylic acid cycle in *Shewanella oneidensis* revealed by Tn-seq. *Mol Microbiol* 86:273–283. <https://doi.org/10.1111/j.1365-2958.2012.08196.x>.
- Heidelberg JF, Paulsen IT, Nelson KE, Gaidos EJ, Nelson WC, Read TD, Eisen JA, Seshadri R, Ward N, Methe B, Clayton RA, Meyer T, Tsapin A, Scott J, Beanan M, Brinkac L, Daugherty S, DeBoy RT, Dodson RJ, Durkin AS, Haft DH, Kolonay JF, Madupu R, Peterson JD, Umayam LA, White O, Wolf AM, Vamathevan J, Weidman J, Impraim M, Lee K, Berry K, Lee C, Mueller J, Khouri H, Gill J, Utterback TR, McDonald LA, Feldblyum TV, Smith HO, Venter JC, Nealson KH, Fraser CM. 2002. Genome sequence of the dissimilatory metal ion-reducing bacterium *Shewanella oneidensis*. *Nat Biotechnol* 20:1118–1123. <https://doi.org/10.1038/nbt749>.
- Wang Z, Leary DH, Malanoski AP, Li RW, Hervey WJ, Eddie BJ, Tender GS, Yanosky SG, Vora GJ, Tender LM, Lin B, Strycharz-Glaven SM. 2015. A previously uncharacterized, nonphotosynthetic member of the *Chromatiaceae* is the primary CO<sub>2</sub>-fixing constituent in a self-regenerating bio-



- cathode. *Appl Environ Microbiol* 81:699–712. <https://doi.org/10.1128/AEM.02947-14>.
40. Ishii T, Kawaiichi S, Nakagawa H, Hashimoto K, Nakamura R. 2015. From chemolithoautotrophs to electrolithoautotrophs: CO<sub>2</sub> fixation by Fe(II)-oxidizing bacteria coupled with direct uptake of electrons from solid electron sources. *Front Microbiol* 6:994. <https://doi.org/10.3389/fmicb.2015.00994>.
  41. Zu Y, Shannon RJ, Hirst J. 2003. Reversible, electrochemical interconversion of NADH and NAD<sup>+</sup> by the catalytic (I<sub>λ</sub>) subcomplex of mitochondrial NADH:ubiquinone oxidoreductase (complex I). *J Am Chem Soc* 125:6020–6021. <https://doi.org/10.1021/ja0343961>.
  42. Hirst J. 2009. Towards the molecular mechanism of respiratory complex I. *Biochem J* 425:327–339. <https://doi.org/10.1042/BJ20091382>.
  43. Spero MA, Brickner JR, Mollet JT, Pisithkul T, Amador-noguez D, Donohue TJ. 2016. Different functions of phylogenetically distinct bacterial complex I isozymes. *J Bacteriol* 198:1268–1280. <https://doi.org/10.1128/JB.01025-15>.
  44. Yang J, Yin L, Lessner FH, Nakayasu ES, Payne SH, Fixen KR, Gallagher L, Harwood CS. 2017. Genes essential for phototrophic growth by a purple *Alphaproteobacterium*. *Environ Microbiol* 19:3567–3578. <https://doi.org/10.1111/1462-2920.13852>.
  45. Gralnick JA, Vali H, Lies DP, Newman DK. 2006. Extracellular respiration of dimethyl sulfoxide by *Shewanella oneidensis* strain MR-1. *Proc Natl Acad Sci U S A* 103:4669–4674. <https://doi.org/10.1073/pnas.0505959103>.
  46. Okamoto A, Hashimoto K, Nealon KH, Nakamura R. 2013. Rate enhancement of bacterial extracellular electron transport involves bound flavin semiquinones. *Proc Natl Acad Sci U S A* 110:7856–7861. <https://doi.org/10.1073/pnas.1220823110>.
  47. Bird LJ, Bonnefoy V, Newman DK. 2011. Bioenergetic challenges of microbial iron metabolisms. *Trends Microbiol* 19:330–340. <https://doi.org/10.1016/j.tim.2011.05.001>.
  48. Edwards MJ, White GF, Norman M, Tome-Fernandez A, Ainsworth E, Shi L, Fredrickson JK, Zachara JM, Butt JN, Richardson DJ, Clarke TA. 2015. Redox linked flavin sites in extracellular Decaheme proteins involved in microbe-mineral electron transfer. *Sci Rep* 5:11677. <https://doi.org/10.1038/srep11677>.
  49. Fieschi F, Nivière V, Frier C, Décout JL, Fontecave M. 1995. The mechanism and substrate specificity of the NADPH: flavin oxidoreductase from *Escherichia coli*. *J Biol Chem* 270:30392–30400. <https://doi.org/10.1074/jbc.270.51.30392>.
  50. Lei B, Tu SC. 1998. Mechanism of reduced flavin transfer from *Vibrio harveyi* NADPH-FMN oxidoreductase to luciferase. *Biochemistry* 37:14623–14629. <https://doi.org/10.1021/bi981841+>.
  51. Tinikul R, Pitsawong W, Sucharitakul J, Nijvipakul S, Ballou DP, Chaiyen P. 2013. The transfer of reduced flavin mononucleotide from LuxG oxidoreductase to luciferase occurs via free diffusion. *Biochemistry* 52:6834–6843. <https://doi.org/10.1021/bi4006545>.
  52. Flynn CM, Hunt KA, Gralnick JA, Srienc F. 2012. Construction and elementary mode analysis of a metabolic model for *Shewanella oneidensis* MR-1. *Biosystems* 107:120–128. <https://doi.org/10.1016/j.biosystems.2011.10.003>.
  53. Pinchuk GE, Hill EA, Geydebekht OV, de Ingeniis J, Zhang X, Osterman A, Scott JH, Reed SB, Romine MF, Konopka AE, Beliaev AS, Fredrickson JK, Reed JL. 2010. Constraint-based model of *Shewanella oneidensis* MR-1 metabolism: a tool for data analysis and hypothesis generation. *PLoS Comput Biol* 6:e1000822. <https://doi.org/10.1371/journal.pcbi.1000822>.
  54. Aleem MI, Lees H. 1963. Adenosine triphosphate-dependent reduction of nicotinamide adenine dinucleotide by ferro-cytochrome c in chemolithoautotrophic bacteria. *Nature* 200:759–761. <https://doi.org/10.1038/200759a0>.
  55. Myers CR, Nealon KH. 1988. Bacterial manganese reduction and growth with manganese oxide as the sole electron acceptor. *Science* 240:1319–1321. <https://doi.org/10.1126/science.240.4857.1319>.
  56. Saville RM, Rakshe S, Haagenen JA, Shukla S, Spormann AM. 2011. Energy-dependent stability of *Shewanella oneidensis* MR-1 biofilms. *J Bacteriol* 193:3257–3264. <https://doi.org/10.1128/JB.00251-11>.
  57. Hau HH, Gralnick JA. 2007. Ecology and biotechnology of the genus *Shewanella*. *Annu Rev Microbiol* 61:237–258. <https://doi.org/10.1146/annurev.micro.61.080706.093257>.
  58. Byrne JM, Klueglein N, Pearce C, Roso KM, Appel E, Kappler A. 2015. Redox cycling of Fe(II) and Fe(III) in magnetite by Fe-metabolizing bacteria. *Science* 347:1473–1476. <https://doi.org/10.1126/science.aaa4834>.
  59. Rowe AR, Chellamuthu P, Lam B, Okamoto A, Nealon KH. 2014. Marine sediments microbes capable of electrode oxidation as a surrogate for lithotrophic insoluble substrate metabolism. *Front Microbiol* 5:784. <https://doi.org/10.3389/fmicb.2014.00784>.
  60. D'Hondt S, Spivack AJ, Pockalny R, Ferdelman TG, Fischer JP, Kallmeyer J, Abrams LJ, Smith DC, Graham D, Hasiuk F, Schrum H, Stancin AM. 2009. Subseafloor sedimentary life in the south Pacific Gyre. *Proc Natl Acad Sci U S A* 106:11651–11656. <https://doi.org/10.1073/pnas.0811793106>.
  61. Picard A, Ferdelman TG. 2011. Linking microbial heterotrophic activity and sediment lithology in oxic, oligotrophic sub-seafloor sediments of the North Atlantic Ocean. *Front Microbiol* 2:263. <https://doi.org/10.3389/fmicb.2011.00263>.
  62. LaRowe DE, Amend JP. 2015. Catabolic rates, population sizes and doubling/replacement times of microorganisms in natural settings. *Am J Sci* 315:167–203. <https://doi.org/10.2475/03.2015.01>.
  63. Jørgensen BB, Boetius A. 2007. Feast and famine—microbial life in the deep-sea bed. *Nat Rev Microbiol* 5:770–781. <https://doi.org/10.1038/nrmicro1745>.
  64. DeShazer D, Woods DE. 1996. Broad-host-range cloning and cassette vectors based on the R388 trimethoprim resistance gene. *Biotechniques* 20:763–764.
  65. Coursolle D, Gralnick JA. 2010. Modularity of the Mtr respiratory pathway of *Shewanella oneidensis* strain MR-1. *Mol Microbiol* 77:995–1008. <https://doi.org/10.1111/j.1365-2958.2010.07266.x>.
  66. Hau HH, Gilbert A, Coursolle D, Gralnick JA. 2008. Mechanism and consequences of anaerobic respiration of cobalt by *Shewanella oneidensis* strain MR-1. *Appl Environ Microbiol* 74:6880–6886. <https://doi.org/10.1128/AEM.00840-08>.
  67. Okamoto A, Hashimoto K, Nakamura R. 2012. Long-range electron conduction of *Shewanella* biofilms mediated by outer membrane C-type cytochromes. *Bioelectrochemistry* 85:61–65. <https://doi.org/10.1016/j.bioelechem.2011.12.003>.
  68. Bretschger O, Obraztsova A, Sturm CA, Chang IS, Gorby YA, Reed SB, Cullley DE, Reardon CL, Barua S, Romine MF, Zhou J, Beliaev AS, Bouhenni R, Saffarini D, Mansfeld F, Kim BH, Fredrickson JK, Nealon KH. 2007. Current production and metal oxide reduction by *Shewanella oneidensis* MR-1 wild type and mutants. *Appl Environ Microbiol* 73:7003–7012. <https://doi.org/10.1128/AEM.01087-07>.
  69. Bücking C, Popp F, Kerzenmacher S, Gescher J. 2010. Involvement and specificity of *Shewanella oneidensis* outer membrane cytochromes in the reduction of soluble and solid-phase terminal electron acceptors. *FEMS Microbiol Lett* 306:144–151. <https://doi.org/10.1111/j.1574-6968.2010.01949.x>.